Journal of Geophysical Research: Oceans

RESEARCH ARTICLE
10.1029/2018JC014103

Observations of the Intermediate Water Exchange Between the South China Sea and the Pacific Ocean Deduced From Transient Tracer Measurements

Hengxiang Deng[1,2], Peng Huang[3], Toste Tanhua[4], Tim Stöven[4], Hongwei Ke[2], Weidong Guo[1,2], Weimin Wang[2], and Minggang Cai[1,2,5]

[1]State Key Laboratory of Marine Environmental Science, College of Ocean and Earth Sciences, Xiamen University, Xiamen, China, [2]College of Ocean and Earth Sciences, Xiamen University, Xiamen, China, [3]College of Ocean and Meteorology, Guangdong Ocean University, Zhanjiang, China, [4]GEOMAR Helmholtz Centre for Ocean Research Kiel, Kiel, Germany, [5]Xiamen Ocean Vocational College, Xiamen, China

Abstract The South China Sea (SCS) is the largest semienclosed marginal sea in the western Pacific (WP) and connects to the west Pacific through the Luzon Strait (LU). In this study, we use the observation of transient tracer chlorofluorocarbon-12 (CFC-12) to calculate the ventilation time scales of the SCS, LU, and WP. The CFC-12 and oxygen data are used together to identify the sandwiched structure vertically of the flows across the LU. The CFC-12 and oxygen distributions reveal a pronounced decrease westward across the LU and a slight decrease southward in the transport of the SCS. The mean age gradient of the salinity minimum (S_{min}) water between the WP and the northern SCS could be a consequence of intensive mixing and entrainment of the inflow water from the WP. An expected difference in age between the LU and SSCS is verified to reflect the transit time for the given water layers in the SCS. Thus, a mean transit time of 77 ± 20 years is estimated for the intermediate water in the SCS interior.

Plain Language Summary In this study, we present CFC-12 data of seawater, which were collected in the South China Sea and western Pacific during September and October 2016. The CFC-12, together with the oxygen and hydrographic data, are used to provide general picture of tracer distributions and ventilation time scales of the South China Sea, Luzon Strait, and western Pacific. The CFC-12 and oxygen data are used together as complementary tracers and identify the sandwiched structure vertically of the flows across the Luzon Strait. We calculate the mean ages using the transit time distributions method to quantify the time scale of waters. An expected difference in age between the Luzon Strait and southern South China Sea is verified to reflect the transit time for the given water layers in the South China Sea. Thus, a mean transit time of ~77 years is estimated for the intermediate water in the South China Sea interior.

Henxiang Deng and Peng Huang contributed equally to this work.

Key Points:
- The CFC-12 and oxygen data are used together to identify the sandwiched structure vertically of the flows across the Luzon Strait
- The ventilation times are estimated for subsurface and intermediate layers in the South China Sea, Luzon Strait, and western Pacific
- The mean transit time of approximately 77 years is estimated for the core of the intermediate water in the SCS interior

Supporting Information:
- Supporting Information S1
- Data Set S1

Correspondence to:
M. Cai,
mgcai@xmu.edu.cn

Citation:
Deng, H., Huang, P., Tanhua, T., Stöven, T., Ke, H., Guo, W., et al. (2018). Observations of the intermediate water exchange between the South China Sea and the Pacific Ocean deduced from transient tracer measurements. *Journal of Geophysical Research: Oceans*, *123*, 7495–7510. https://doi.org/10.1029/2018JC014103

Received 21 APR 2018
Accepted 24 AUG 2018
Accepted article online 4 SEP 2018
Published online 23 OCT 2018

1. Introduction

The South China Sea (SCS), surrounded by the places with high population density and economic activites (e.g., Cai et al., 2017), is one of the largest semienclosed marginal seas in the western Pacific (WP) and connects with the west Pacific through the Luzon Strait (LU) at a sill depth of approximately 2,000 m. Below the sill, there is no direct water exchange between the SCS and the surrounding oceans. As a result, the characteristics of the deep water in the SCS are similar to the Pacific at the depth of 2,000 m (Nitani, 1972; Qu, 2002). This means that the deep SCS water is strongly influenced by the Pacific water. All the other channels connecting the SCS with the surrounding oceans are shallower than the LU and often narrow. Thus, the water exchange between the SCS and the Pacific through the LU is important to both the heat and the salt budgets of the basin (Qu et al., 2009). Generally, there is a sandwiched vertical structure in the water transports through the LU (Chen & Huang, 1996; Li & Qu, 2006; Qu, 2002; Xu & Oey, 2014); the shallow and the deep waters flow into the SCS, while the intermediate water flows out to the Pacific. However, the depth of the intermediate outflow is still controversial (Chen et al., 2001; Li & Qu, 2006; Tian et al., 2009).

The SCS shallow layer circulation and the seasonal variability for the sea surface height (e.g., Xu & Oey, 2015) have been investigated previously. Based on early hydrographic observations, Wyrtki (1961) demonstrated that waters enter the SCS in winter and flow back to the Pacific in summer in response to the seasonally reversing monsoon. Generally, a cyclonic circulation occurs in the winter and an anticyclonic circulation

occurs in the summer (Chu et al., 1999; Chu & Li, 2000; Fang et al., 2009; Liu et al., 2001; Qu, 2000; Shaw et al., 1999; Wyrtki, 1961; Xue et al., 2004). However, few studies have focused on the SCS intermediate and deep circulations. The analysis of water property distributions in the deep SCS reveals a basin-scale cyclonic circulation at depths from approximately 2,400 m to the bottom, which allows Pacific water characteristics to spread southwestward along the continental margin off Southeast China and has a notable impact on the water characteristics of the entire northern SCS (NSCS; Qu et al., 2006; Tian et al., 2006).

Wang et al. (2011) suggested that the cyclonic circulation is mainly forced by the Luzon overflow, with the bottom topography playing an important role. It has been speculated that strong diapycnal mixing in the LU and SCS sustains the baroclinic pressure gradient across the LU, which is the primary driving mechanism of the Luzon overflow (Wang et al., 2017; Zhao et al., 2014) and regional upwellings in the deep SCS (Qu et al., 2006). The North Pacific Deep Water overflows through the LU in the deep layer (Chang et al., 2010; Tian et al., 2006) and is gradually mixed by a strong turbulence generated by the dissipation of internal tides (Tian et al., 2009), and the SCS water eventually exits the SCS in the intermediate layer through the LU (Chao et al., 1996; Chen & Huang, 1996; Qu, 2000; Tian et al., 2006) and in the shallow layer through the Karimata, Mindoro, and Taiwan straits (Qu et al., 2009; Yaremchuk et al., 2009). This unique circulation pattern, with an inflow from the west Philippine Sea in the shallow and deep layers, but an outflow to the west Philippine Sea in the intermediate layer makes the SCS a perfect site to examine ocean margin-open ocean interactions.

As documented by previous studies, the major water masses in the SCS can be identified well based on salinity features (Li et al., 2002; Qu et al., 2000; Zeng et al., 2016). However, as a conventional tracer, salinity cannot be used to track the water transport time scale or the water age. In some studies, a so-called passive tracer (Liu et al., 2016), which is a hypothetic ideal tracer for modeling, has been applied to identify water transports. Some studies have also drawn conclusions using box models and/or mass balance studies based on observed chemical tracers such as carbon parameters, oxygen, and nutrients (e.g., Chen et al., 2001; Chen & Huang, 1996; Dai et al., 2009; Wu et al., 2015).

Measurements of chemical tracers with time-varying input functions can provide information on water transport time scales in the ocean. As on class of conserved "chronological tracers (i.e., transient tracers)" in the ocean, chlorofluorocarbons (CFCs) have adequate time-dependent source functions and are widely used to understand annual to decadal oceanic processes such as ocean circulation (e.g., Rhein, 1994; Smethie et al., 2000), the rates and variability of water mass formation (e.g., Hartin et al., 2011; LeBel et al., 2008; Orsi et al., 1999; Rhein et al., 2002; Smethie & Fine, 2001), upper ocean ventilation (e.g., Deng et al., 2018; Sonnerup et al., 2008; Tanhua & Liu, 2015), and the estimation of biogeochemical rates, including apparent oxygen utilization rates (e.g., Mecking et al., 2004; Sonnerup et al., 1999; Warner et al., 1996) and anthropogenic CO_2 (C_{ant}) inventories (e.g., Gruber et al., 1996; Sabine et al., 2004; Tanhua et al., 2009; Waugh et al., 2006).

Comparatively, few studies based on CFCs and/or sulfur hexafluoride (SF_6) have been carried out in Southeast Asian seas, including the SCS. Fieux et al. (1996) studied the Indonesian throughflow based on measured CFC data, and Waworuntu et al. (2000) studied the pathway of inflow water from the WP Ocean to the Banda Sea using CFC-11 data. Recently, Huang and Tanhua (2017) studied ventilation and C_{ant} storage of the Sulu Sea using measurements of SF_6 and CFCs. Observations of CFCs in the SCS are spare, though Sun (2006) studied the CFC distribution and the partial pressure age based on the limited data. Recently, Huang et al. (2016) reported a CFC-11 data set in the SCS, and the ventilation time and C_{ant} were first estimated based on the transit time distributions (TTDs) method, which were in agreement with the previous results. However, the transient tracer data in the SCS are still too sparse to accurately characterize the ventilation time scales and circulation pattern of the SCS. Thus, it is important to obtain more transient tracer data in the SCS.

In this paper, we present observations of the transient tracer CFC-12 in the SCS, LU, and WP east of LU during the fall of 2016. With the transient tracer CFC-12 data and oxygen as complementary tracer, this study provides a general picture of the tracer distribution in the LU and SCS. As far as we know, this is the first time that transient tracer data have been obtained across the LU, which gives us useful differences among not only the physical but also the chemical parameter (e.g., CFC-12) features. Thus, it is possible to provide a ventilation time scale and transit time along the water exchange pathway between the NSCS and the WP. The rest of this paper is organized as follows: The data and methods of the analysis are described in section 2; section 3 presents the results, which are then discussed in section 4 and summarized in section 5.

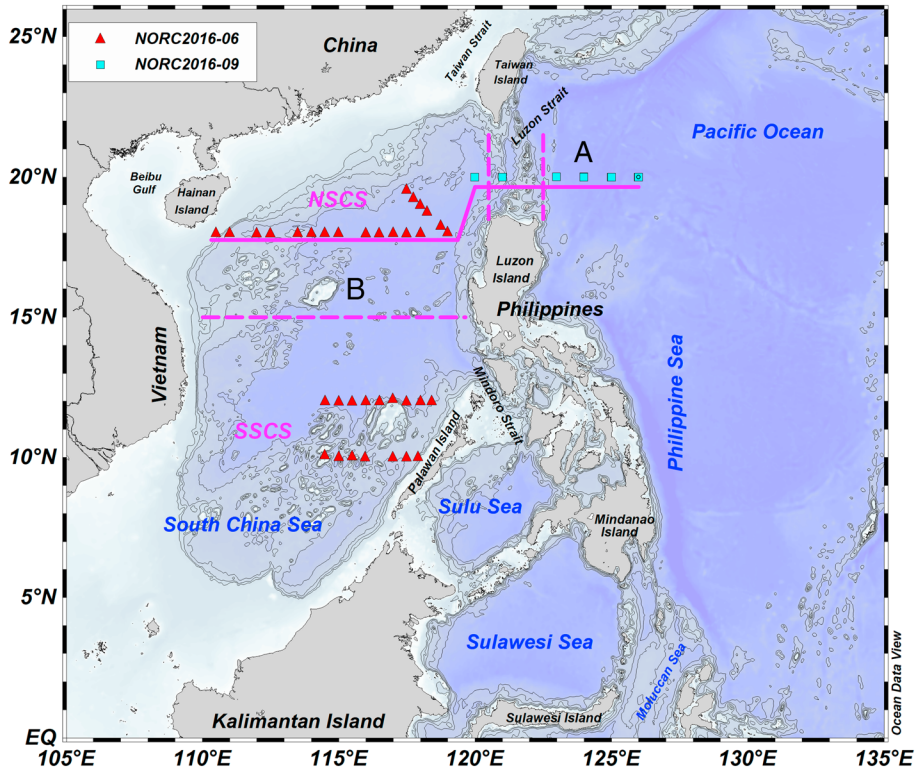

Figure 1. Station map of the South China Sea (SCS), Luzon Strait, and Pacific Ocean. The depth contours are 250, 500, 1,000, 2,000, and 3,000 m. The stations marked with magenta lines A and B will be discussed in detail later. SSCS, NSCS, and WP indicate the southern SCS, northern SCS, and western Pacific, respectively. The 15°N dashed thick line indicates the signal line that separates the SCS into the NSCS and SSCS. The 120.5°E and 122.5°E dashed thick lines indicate the signal lines that separate the Luzon Strait from the SCS and WP.

2. Materials and Methods

2.1. Sampling and Tracer Measurements

During the fall of 2016, two cruises were undertaken to the SCS, LU, and WP: One cruise was with the R/V SHIYAN I (Cruise ID: NORC2016-06) in August and September, and the other was with the R/V KEXUE (Cruise ID: NORC2016-09) in September and October. The sampling stations are shown in Figure 1. All the samples for the analysis of CFCs were collected with 300-mL glass ampoules and were flame sealed under a flow of ultrahigh purity nitrogen (Busenberg & Plummer, 1992; Vollmer & Weiss, 2002), which allows the samples to be measured onshore. The CFC-12 and SF_6 were measured simultaneously in the laboratory using a purge and trap GC system (Cai et al., 2016; Stöven, 2011).

Since we use a customized cracker for ampoule breaking and purging, a blank for the cracker must be determined without breaking the ampoule. The result showed undetectable amounts of CFC-12 and SF_6. Then the system detection limits were estimated to be 0.005 pmol/kg for CFC-12 and 0.03 fmol/kg for SF_6 by 3 times the standard deviation of the noise level. A small blank of 0.02 pmol/kg for CFC-12 was obtained, that is, probably traces of air introduced to the sample during sampling, flame sealing, and ampoule breaking by the cracker in the lab. Although no replicate seawater samples were taken during the cruises, the analytical precision of this setup was on the order of ±3% or 0.03 pmol/kg for CFC-12, whichever is greater. Due to the unforeseen contaminations, which might be from the Niskin, SF_6 cannot be used in this study. Dissolved oxygen (DO) data used in this study was measured using Winkler technique with photometric endpoint detection with a precision of 0.7 μmol/kg or 0.3%.

The CFC-12 concentrations (in pmol/kg) were converted to the partial pressure in ppt (i.e., parts per trillion) using solubility functions (Bullister et al., 2002; Warner & Weiss, 1985). This is to eliminate the effects of temperature and salinity on the tracer solubility, and the derived partial pressures of the tracers can be compared

directly to their time-varying atmospheric histories (Bullister, 2015) to determine the tracer age and the so-called TTDs, as shown in the details below.

2.2. Water Age Calculation

Typically, the "tracer age" concept is assumed, where the water parcel is uniform and no mixing with the surrounding waters takes place. From the above "chronological" tracers, that is, CFC-12 here in this study, it is possible to define a tracer age as the elapsed time since the surface concentration was equal to the interior concentration. Actually, the ocean interior mixing can lead to substantial biases (Beining & Roether, 1996). Thus, the ideal tracer age is not realistic if it is derived directly from the atmospheric history of the tracer. One way to obtain a true ventilation age is by using the TTD method (Waugh et al., 2003). According to this method, the mean age can be calculated for the water samples.

The TTD method assumes that a water mass consists of many different ages or transit times. The ocean interior concentration $C(r, t)$ of the tracer at location r and time t can be expressed as follows in the case of steady state conditions:

$$C(r,\ t) = \int_0^\infty C_0\left(t - t'\right) G\left(r,\ t'\right) dt' \tag{1}$$

where t' is the integration variable (ranging from 0 to ∞ years); $G(r, t')$ is the TTD at location r and time t'; and $C_0(t - t')$ is the surface water tracer concentration in the year $t - t'$. If the steady state is valid, the TTD can be computed assuming that the inverse Gaussian (IG) form of the TTD is a valid representation of the 1-D flow and mixing:

$$G\left(t'\right) = \sqrt{\frac{\Gamma^3}{4\pi\Delta^2 t'^3}} \exp\left[\frac{-\Gamma\left(t' - \Gamma\right)^2}{4\Delta^2 t'}\right] \tag{2}$$

where Γ and Δ are interpreted as the mean and width of the TTD. The different Δ/Γ ratios represent the different patterns of diffusion and advection processes. The larger ratio of Δ/Γ means stronger mixing and vice versa. In principle, one could measure two transient tracers (such as CFC-12 and SF_6) with distinct histories simultaneously and then put constraints on the Δ/Γ ratio. For the SCS, LU, and WP, the shape of the Δ/Γ ratio can only be assumed since we do not have SF_6 (or any other independent tracer) data to empirically constrain the ratio. Thus, a ratio of 1 was applied in this study since it is appropriate for most of the ocean thermoclines (Waugh et al., 2004). Care must be taken that the IG-TTD is a simple approximate to the water flows. For real transport in the ocean, it cannot be completely treated as an ideal 1-D flow (Khatiwala et al., 2012).

3. Results

3.1. Hydrography Data

The vertical profiles of potential temperature and salinity in the SCS, LU, and the adjacent Pacific Ocean are presented in Figure 2. The properties of the water in the upper 2,000 m are different for the SCS and the adjacent WP Ocean. Salinity is plotted against the potential temperature in Figure 3. As a result, the plot clearly reveals that there is a significant reversed "S"-shaped T-S relationship, that is, high temperature and low salinity for the surface layer (<30 m); high temperature and high salinity for the subsurface layer (core at ~150–200 m); low temperature and low salinity for the intermediate layer (core at ~400–600 m); and low temperature and high salinity for the deep layer (>~1,500 m).

The salinity maximum water is the signature of the North Pacific Tropical Water (NPTW; Nitani, 1972; Suga et al., 2000). Down to the depth of approximately 400 m, the salinity minimum zone located in the σ_θ range of 26–27, which is regarded as the intermediate water that originated from the North Pacific Intermediate Water (NPIW; Qu et al., 1999; Qu et al., 2000; Wyrtki, 1961; You et al., 2005). For the deep water, the salinity and the potential temperature values in the SCS are homogeneous and similar to those in the LU and Pacific, indicating that the deep water in the SCS originated from the North Pacific Deep Water (e.g., Chen et al., 2006; Gong et al., 1992).

As shown in Figure 3, the Pacific water (see red line) has an intermediate layer salinity minimum of ~34.18 contrasted to the subsurface layer salinity maximum of ~35.08. The existence of a salinity maximum and

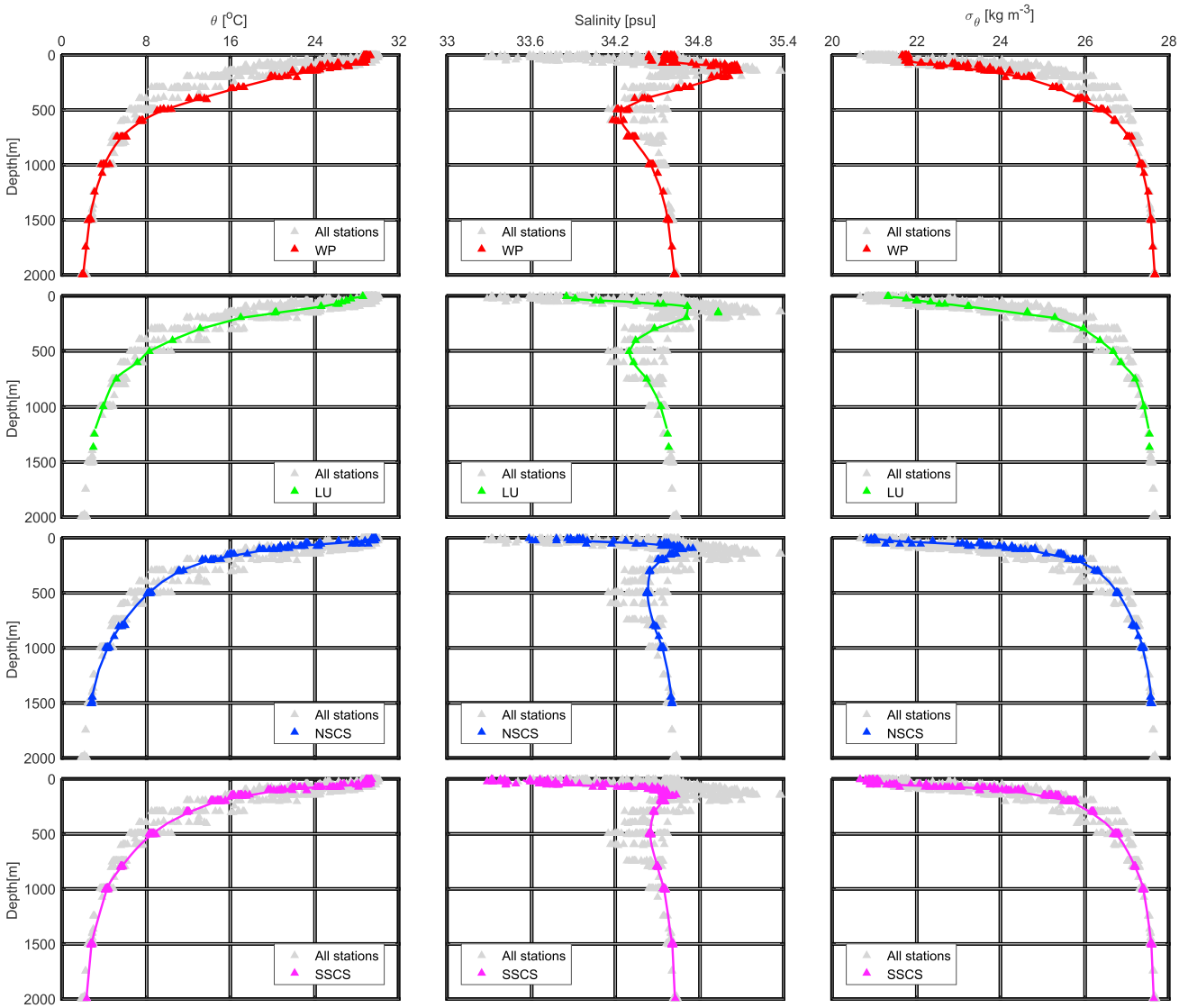

Figure 2. Vertical profiles of potential temperature (θ [°C]; left column), salinity (psu; middle column), and potential density (σ_θ [kg/m^3]; right column). The gray dots represent the data for all stations. The red lines represent the mean profiles of the given parameters in the western Pacific (longitude > 121°E), the green lines represent the mean profiles of the given parameters in the Luzon Strait (i.e., the station between 120.5°E and 122.5°E), the blue lines represent the mean profiles of the given parameters in the NSCS (i.e., the stations along 18°N), and the magenta lines represent the mean profiles of the given parameters in the SSCS (i.e., the stations along 10°N and 12°N). The gray dots represent all the data points. NSCS = northern South China Sea; SSCS = southern South China Sea; LU = Luzon Strait; WP = western Pacific.

minimum in the SCS and the resemblance between the waters of the two seas reflect the influence of water intrusion from the west Pacific to the SCS. As the salinity minimum is conserved up to a σ_θ of 26.7 (~500 m), the strong temperature and salinity gradients along the LU did not induce a large change in the density (Figure 3), that is, the core density of NPIW is still stable. If we focus on the interior of the SCS from north to south, the salinity maximum and minimum gradually became weaker, reaching a maximal value of 34.60 and minimal value of 34.45 in the southern SCS (SSCS). However, despite that relative weakness of ventilation in the SSCS, the salinity extremes can still be seen in most parts of the SCS. Thus, intensive upwelling and vertical mixing tend to reduce the extreme signals in the NSCS (Chen & Huang, 1996).

3.2. CFC-12 Data

Figure 4 shows the CFC-12 profiles for all the stations. As shown in Figure 4, detectable concentrations of CFC-12 are found throughout the water column from the surface to the depth of ~1,500 m, with CFC-12

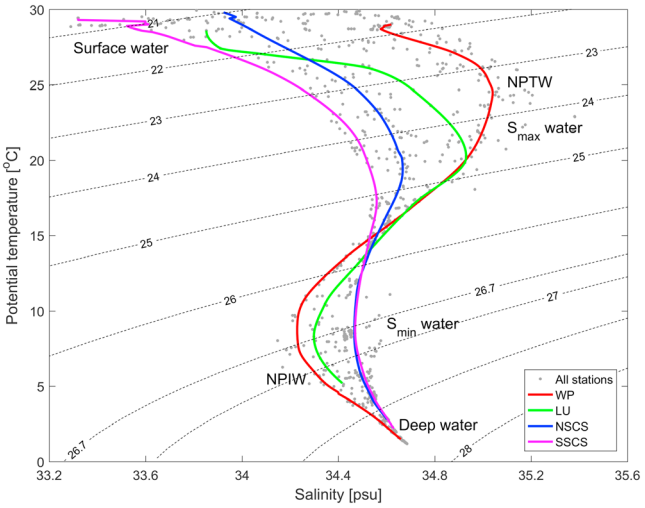

Figure 3. T-S diagram of the stations in the South China Sea, Luzon Strait, and Pacific Ocean. The lines with different colors refer to the legend in Figure 2. S_{max} water and S_{min} water represent the salinity maximum of the water and salinity minimum of the water, respectively, while NPTW and NPIW represent North Pacific Tropical Water and North Pacific Intermediate Water, respectively. NSCS = northern South China Sea; SSCS = southern South China Sea; LU = Luzon Strait; WP = western Pacific.

concentrations at or below the detection limit (i.e., ~0.005 pmol/kg) in the deeper layers. The CFC-12 concentration in the surface water (<~30 m) is in equilibrium with the contemporary atmospheric CFC-12 concentration (~520 ppt, converted to the partial pressure). Below the warm surface layer, in general, there is a CFC-12 subsurface maximum lying at the depth of ~200 m. This subsurface CFC-12 maximum core corresponds to the well-defined salinity maximum as mentioned in section 3.1 and can be tracked to the NPTW (Nitani, 1972). Below the subsurface layer, the CFC-12 decreases monotonically with depth to the bottom, although there are some differences among WP, LU, and SCS (Figure 4).

Below the depth of ~100 m, the CFC-12 concentration is higher in the WP than that in the LU, which, in turn, is higher than that in the SCS. The CFC-12 vertical distributions throughout the water columns in the SCS, however, show different trends compared with those in the WP zone. Since the LU is the portal for the water exchange. To determine the detail of the water exchange between the WP and SCS, a section of selected parameters along NSCS-LU-WP and SSCS is sequentially plotted in Figures 5 and 6, respectively.

For stations in the WP, as part of the western boundary of the subtropical gyre, a CFC-12 maximum core can be seen in the upper 400 m depth, covering the subsurface layer (i.e., $24 < \sigma_\theta < 26$). While, a thinner and less remarkable CFC-12 maximum core in the NSCS also can be found in a shallower depth of ~150 m. Due to the lack of direct vertical convection process in the SCS itself allowing prominent CFC-12 enter the basin. Below the main thermocline, although CFC-12 concentration is still higher in the WP than in the SCS, there is no significant spatial difference between these regions. In contrast, owing to the geological and topographical conditions acting like a "bottleneck," the SSCS had weak water exchange, and it is expected that the relatively low CFC-12 concentration could be observed below the mixed layer (as shown in Figure 6a).

Generally, the CFC-12 distribution reveals a pronounced east-west change across the LU and then varied slightly southward in the SCS (Figure 5a). The high-CFC-12 water on the Pacific side might reflect the water characteristics of the previous winter or be a result of the predominance of evaporation in the subtropical North Pacific. In the LU, the CFC-12 vertical distribution indicated LU water is a mixture of WP and SCS water. It is noteworthy that the CFC-12 vertical distribution of the SCS is more uniform than that of the WP in the water column below the subsurface layer. This may result from vertical mixing, and the result supports the earlier speculation of the vitally important dynamic role of mixing in controlling the water mass properties and circulation structures in the SCS (Wang et al., 2017).

The spatial difference of CFC-12 maximum core indicates that waters with high CFC-12 concentrations are probably carried westward from the WP to the SCS through LU. In addition, the trends and differences between the SCS and WP also manifest that the vertical advection of cold deep water in the SCS must occur. Thus, it is possible that CFC-12-free deep water could be carried upward and dilute CFC-12 concentration in the upper layers.

3.3. Mean Age of Water

As described in section 3.2, The CFC-12 distributions show regional concentration gradients from WP westward to the NSCS across the LU and then to the SSCS southward. The subsurface CFC-12 maximum core in the SCS is relatively less conspicuous than that in the WP. However, the tracer concentration distribution only gives us a general snapshot, showing the features qualitatively. To put some constraints on the time scale quantitatively, the TTD method is used with CFC-12 data to derive the mean age. Details of error analysis will be discussed in section 4.3.

Figure 4 shows the vertical distribution of the mean age for all stations. Though one should notice that an additional complication arises from the decreasing atmospheric CFC-12 concentrations since the mid-2000s, and CFC-12 cannot provide inconclusive ventilation information for the recent decades. That is, for

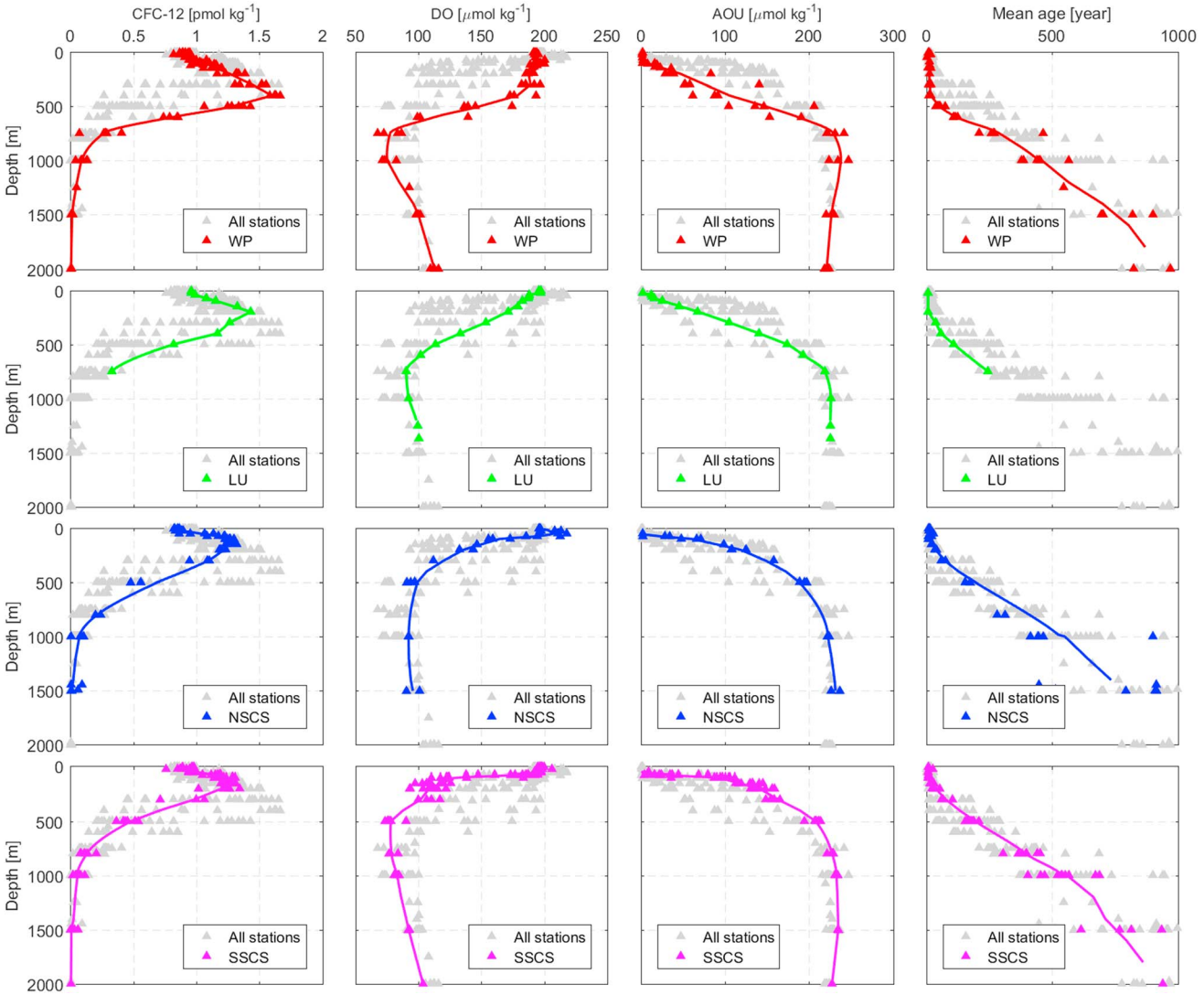

Figure 4. Vertical profiles of CFC-12 (pmol/kg; first column from the left), DO (μmol/kg; second column from the left), AOU (μmol/kg; third column from the left), and mean age (year; fourth column from the left) in the South China Sea, Luzon Strait, and Pacific Ocean. The gray triangles represent the data for all stations. The lines with different colors refer to the legend in Figure 2. NSCS = northern South China Sea; SSCS = southern South China Sea; LU = Luzon Strait; WP = western Pacific; CFC = chlorofluorocarbon; DO = dissolved oxygen; AOU = apparent oxygen utiliztion.

the upper layer (<~100 m), the mean age could be any value from 0 to ~20 years. Below the surface layer, the mean age increases monotonically with depth throughout the entire water column at all the stations. The mean ages exceed 400 years below the depth of ~1,000 m, where the concentrations of CFC-12 are close to the limit of detection, and any estimates of mean age cannot be resolved with the given CFC-12 data. Meanwhile, there is a mean age gradient along the transect from the WP to the NSCS and then to the SSCS at the upper 700 m depth (Figure 4). The quantitative description will be held in section 4.1 and 4.2.

3.4. Oxygen Data

As a componence for CFC-12, oxygen will be used to describe the water below subsurface layer where extremely low CFC-12 signal cannot be used to provide effective information. The DO profile of the SCS has a remarkable decrease from ~200 μmol/kg in the mixed layer (<30 m) to ~130 μmol/kg at the depth of 100 m (Figure 4). Below the depth of ~100 m, oxygen decreases gradually to a minimum of ~80 μmol/kg at a depth of ~600 m and then increases with depth down to the bottom. These vertical distributions are apparently different from those in the WP, where the oxygen shows only a small decreasing trend in the

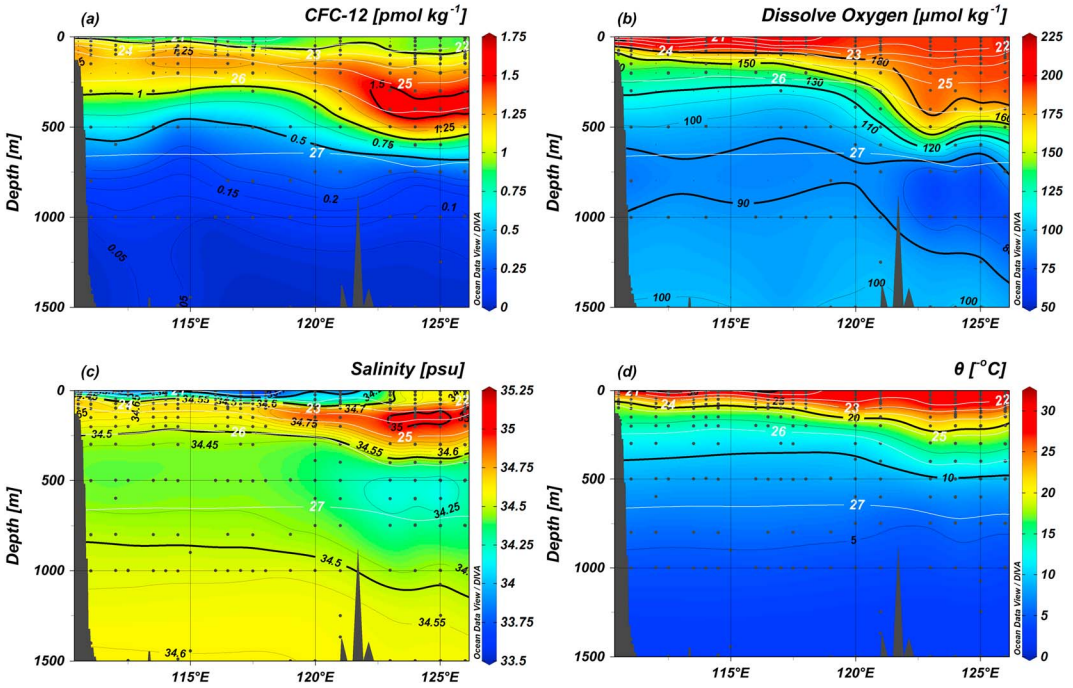

Figure 5. Upper 1,500-m vertical sections of CFC-12 (a), dissolved oxygen (b), salinity (c), and potential temperature (d) for the stations across the Luzon Strait (the magenta section band A in Figure 1). The white contour line overlay represents the potential density isopycnals. CFC = chlorofluorocarbon.

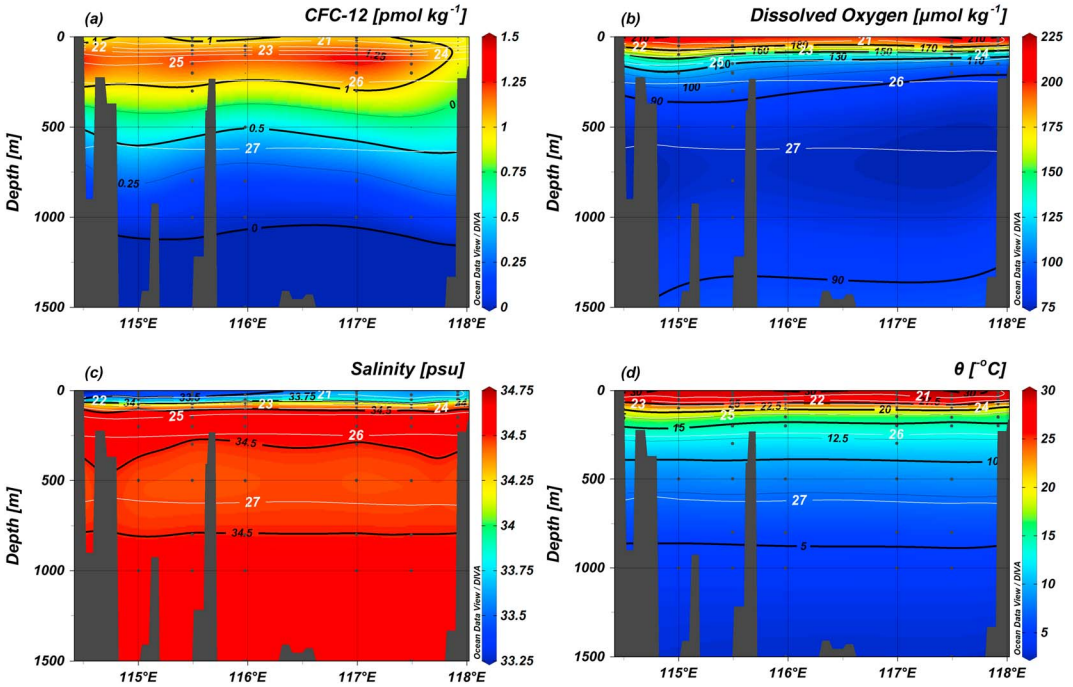

Figure 6. Upper 1,500-m vertical sections of CFC-12 (a), dissolved oxygen (b), salinity (c), and potential temperature (d) for the stations in the SSCS (magenta section band B in Figure 1). The white contour line overlay represents the potential density isopycnals. CFC = chlorofluorocarbon.

upper 400 m. A minimum core of ~80 μmol/kg is found at ~1,000 m, and then the oxygen increases toward the bottom.

As can be seen in Figure 5b, the horizontal variation in oxygen is largest in the intermediate layer. Similar to the CFC-12, the oxygen distribution also shows a gradual decreasing trend in the upper 700 m depth along the transect line from the WP to the SSCS across the LU, as expected in the mixed layer. This result agrees well with the previous studies (e.g., Chen & Huang, 1996; Li & Qu, 2006; Qu & Lindstrom, 2004), manifesting that the oxygen-rich upper water originated from the Pacific Ocean. Below the depth of ~700 m, the oxygen in the SCS is higher than that in the WP. For the depths greater than ~1,400 m, again, the oxygen in the WP is higher than that in the SCS. The existed dissolved oxygen minimum (DO_{min}) at around 700 m indicates that this water is the oldest in the SCS, which lies between the relatively young waters above and deep water below.

It is obvious from Figure 5b that a low-oxygen water from the WP (80–90 μmol/kg contour) can be found east of 125°E along the section. In the NSCS, the DO_{min} core is less significant than that in and outside LU. The strong vertical mixing in the NSCS is responsible for high oxygen values in the intermediate SCS waters (Figure 4). Large solitary internal waves move through the LU and break in NSCS, which causes strong mixing (Warn-Varnas et al., 2010). If we focus on the southern part in the SCS (Figure 6b), DO_{min} core expands and becomes thicker compared to the northern part in the SCS. Even we can see the oxygen minimum core, it weakens rapidly inside the SCS from the north to the south.

The vertical distribution of oxygen clearly manifests the existence of intermediate water advection between the SCS and the Pacific (Figure 5b), supporting the previous studies that found outflow to be more important in the intermediate water (Tian et al., 2006; Xue et al., 2004). The oxygen distributions also support the earlier speculation that the oxygen-rich abyssal water is from the Pacific (e.g., Qu & Lindstrom, 2004; Wang, 1986; Wyrtki, 1961), though data for only the upper 2,000 m are obtained.

4. Discussion

4.1. Spatial Distribution of Mean Age

Considering that the water tends to flow along the isopycnals, the averaged CFC-12 and mean age profiles versus potential density are plotted in Figures 7 and 8. Plots with potential density identify differences better than those with depth only. As shown in Figure 7, there are significant gradients of CFC-12 in the intermediate layer among WP, LU, NSCS, and SSCS, where the potential densities range from 25 to 26.7. We also compare the mean age difference between the WP and SCS at the same isopycnals (Figure 8). For the water with $\sigma_\theta < 26.7$ (approximately 600 m, Figure 2), the WP water is younger than the LU water, while for the water with $\sigma_\theta > 26.7$, the WP water is relatively old. Along WP, LU, NSCS, and SSCS, sequentially, a gradual decrease in CFC-12 and a gradual increase in the mean age are observed within the upper intermediate layer ($24.8 < \sigma_\theta < 26.7$), indicative of its Pacific origin.

For the station in the LU (i.e., station 4 shown in Figure 1), the average mean age of the S_{max} water (~150 m or $\sigma_\theta = 25$) is ~20 years (with higher uncertainty due to the decline in CFC-12), while the S_{min} water (~500 m or $\sigma_\theta = 26.7$) is ~113 ± 31 years. For water deeper than 500 m, the mean ages continue to increase with depth until the value exceeds 400 years at ~1,000 m. For the stations along 18°N (i.e., NSCS), similarly, the mean age of S_{min} water rapidly increases to 147 ± 41 years. This must be the consequence of intensive entrainment for the inflow water from the WP. A similar tendency is also found in the stations along 10°N; the S_{min} water (~500 m or $\sigma_\theta = 26.7$) is 191 ± 53 years, though with a large uncertainty.

Such higher mean ages demonstrated that the intermediate water must ventilated from the region that far away from the SCS, that is, North Pacific (e.g., Qu, 2002; Qu et al., 2006; You et al., 2005). That means a longer ventilation time of the intermediate would be expected, which is consistent with the result from oxygen that the intermediate water is the oldest.

4.2. Age Difference Below the Subsurface Layer in the SCS

According to the T-S relationship (Figures 2 and 3) and tracer distributions (Figures 5 and 6), the densities $\sigma_\theta = 24$ and $\sigma_\theta = 26$ were selected to represent the upper and lower boundary of the subsurface layer, respectively. $\sigma_\theta = 26.7$ was selected to represent the core of the intermediate water, and $\sigma_\theta = 27$ was set as the lower

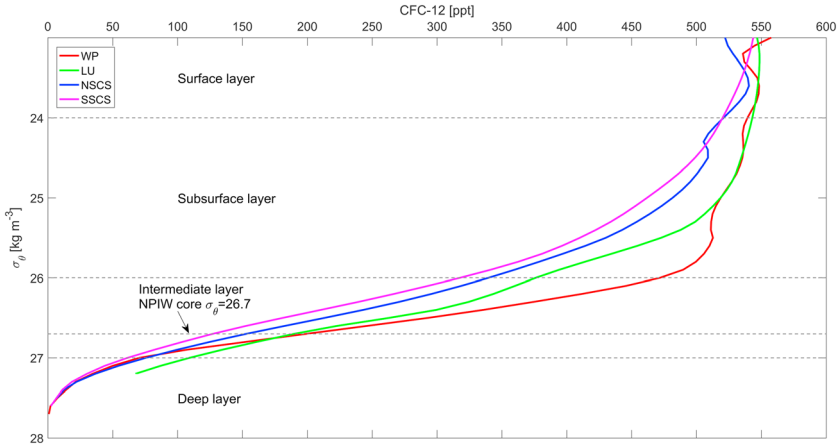

Figure 7. Average vertical profiles of pCFC-12 (ppt) versus potential density (kg/m^3) for the given regions. The lines with different colors refer to the legend in Figure 2. NSCS = northern South China Sea; SSCS = southern South China Sea; LU = Luzon Strait; WP = western Pacific; CFC = chlorofluorocarbon; NPIW = North Pacific Intermediate Water.

boundary of the intermediate water in the SCS. We then focused on the intermediate water (i.e., $26 < \sigma_\theta < 27$).

Since the age of water have many definitions and applications. It is important to clarify the differences between transit time (or residence time) and ventilation time (i.e., mean age) that we are reporting based on CFC-12 data. The ventilation time refers to the elapse time since the water parcel was in contact with the atmosphere whereas the residence time refers to the time the water parcel spends in a bulk space. If the water already has a nonzero ventilation age entering a given area, it could be expected that the ventilation time to be higher than the transit time. Thus, these two concepts of ages are complimentary and provide information of two different ways.

In fact, we do expect the inflowing water from the WP to have considerable CFC-12 concentrations, that is, to have a nonzero ventilation time, which has been confirmed by our tracer data. In our previous study, Huang et al. (2016) provided CFC-11 distributions in the SCS basin and estimated the ventilation time scale for the SCS waters. However, it is only a basic and sketchy study that no any data collected in the LU. Fortunately, we do have trace data in the LU to verify this. So that an expected increase in age between the LU and SCS could be verified, that is, to reflect the transit time of the water in the SCS. The LU is set as a reference point, and the SSCS as the southern end. Then the mean age differences are estimated to be 23–122 years

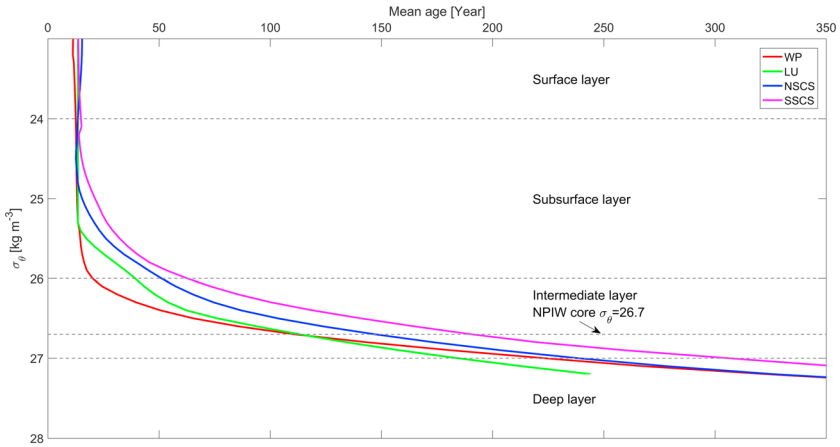

Figure 8. Average vertical profiles of mean age (year) versus potential density (kg/m^3) for the given regions. The lines with different colors refer to the legend in Figure 2. NSCS = northern South China Sea; SSCS = southern South China Sea; LU = Luzon Strait; WP = western Pacific; NPIW = North Pacific Intermediate Water.

for the intermediate water ($26 < \sigma_\theta < 27$), with a mean value of 77 ± 20 years for its core ($\sigma_\theta = 26.7$). Thus, this can be regarded as the mean transit time for the intermediate water below the subsurface layer in the SCS interior. This result is well matches the previously estimates based on hydraulic theory and chemical tracers (e.g., Broecker et al., 1986; Chen & Huang, 1996; Chen et al., 2001; Gong et al., 1992; Qu et al., 2006; Yang et al., 2011) since the upper limit of 100 years of the residence time was documented, but longer than the result by Liu and Gan (2017).

The age differences can be explained by the fact that the SCS is a cul-de-sac for the subtropical NPIW (You et al., 2005). As mentioned above, tracer data could verify a sandwich structure. That means a reversed age trend would be expected, that is, younger in the SCS interior and older in the LU as a reference. However, it appears that we cannot find a reversed age trend based on our age data. A reasonable explanation is that the inflow under the winter monsoon is stronger than the outflow under the summer monsoon, which leads to a net annual transport of NPIW into the SCS. Thus, tracers could continuously enter the SCS which are carried by the annual mean inflow.

4.3. Error Analysis for Age Estimate

4.3.1. Major Error Sources for TTD Approach

Briefly, the age estimation contains uncertainty including analytical errors, degree of tracer saturation, and Δ/Γ ratios (i.e., assumptions made on the parametrization of the TTD). Details of how these errors are estimated can be referenced in, for example, Tanhua et al. (2008).

Figure 10 shows the profiles of all estimated mean ages with the error ranges. Apart from the error in the tracer measurement, some assumptions made for the TTD method lead to uncertainties in the water mass ages, such as uncertainties in the initial degree of saturation of the tracers, uncertainties in the atmospheric history, and the assumption of an IG distribution with a Δ/Γ ratio of one (Tanhua et al., 2008).

The analytical precision of our method is usually on the order of ±3% or 0.03 pmol/kg for the CFC-12 measurement, whichever is greater. In this method, 100% saturation of CFC-11 is assumed for the calculation. However, a lower saturation may be possible for the waters that do not originate in the tropics or subtropics (Fine, 2011). Here a lower limit for the tracer saturation (a value of 80%) was chosen. A saturation degree larger than 100% is unlikely since it might only occur during the time period of rapid warming of the surface water.

4.3.2. Sensitivity of the TTD Shape

In this study, a uniform Δ/Γ ratio of 1 (Waugh et al., 2003) for all samples is applied for mean age calculation. However, the ratio of 1 is still an empirical value since we do not have the second transient tracer with different input histories except CFC-12. One should know that the TTD method is extremely sensitive to the Δ/Γ ratio. Figure 9a shows the model output of the CFC-12 concentrations and ages using TTD approach. The theoretical CFC-12 concentrations were calculated for Δ/Γ ratios between 0 and 2.0 and a mean age spectrum between 0 and 2,000 years. Such theoretical tracer concentrations can then be interpolated to measured concentrations, which yields the different mean age results for given ratios. Thus, each tracer has a specific time and application range as shown in Figure 9a. It can be found in Figure 9a that the given ratios yield a broad mean age range, especially for lower tracer concentrations, that is, intermediate and deep water. That is the reason why a scattered distribution of mean age for deep water could be found as shown in Figure 10.

On the other hand, for small Δ transport is dominated by advection, and the TTD is narrow and peaked near the mean age. $\Delta = 0$ corresponds to pure advection and a delta function TTD at tracer age t (see section 2.2) equal to Γ. As Δ is increased (diffusion increased) the TTD broadens, which means that it encompasses a broad range of transit times (Waugh et al., 2003, 2004). In other words, weaker mixing ($\Delta/\Gamma < 1$) results in younger ages and stronger mixing ($\Delta/\Gamma > 1$) results in older ages.

According to the previous studies advection and upwelling might also play an important role for water transport in the SCS. Consequently, a lower Δ/Γ ratio would be more realistic in the SCS. Recently, Liu and Gan (2017) used the WORLD OCEAN ATLAS 2013 (WOA13) hydrographic data and China Sea Multi-Scale Ocean Modeling System (CMOMS) model to investigate the pathways and ages of water masses in the SCS. Their result reveals that the longest residence time of ~42 years could be found in the intermediate water. Liu and Gan's result, which is supported by the spatial variation in the observed potential density, though, it is shorter than our estimate based on TTD method with Δ/Γ ratio of one.

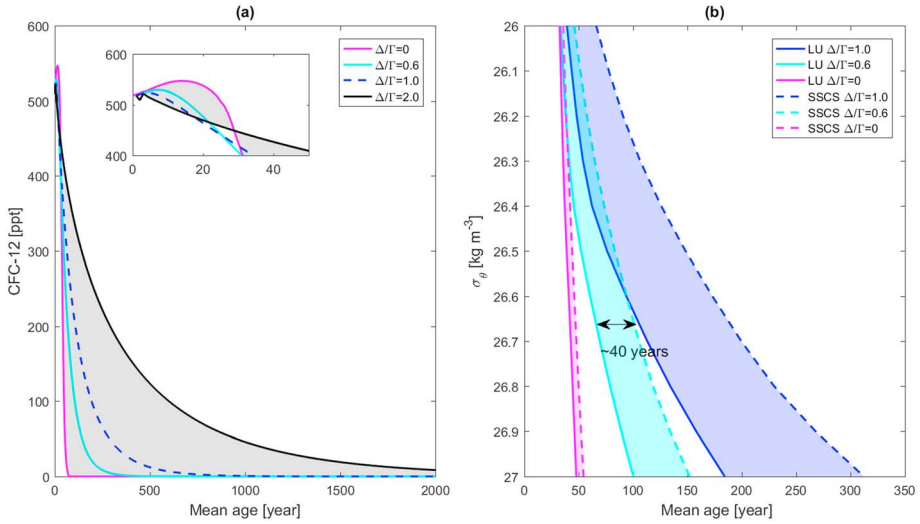

Figure 9. (a) CFC-12 concentration (in ppt) versus mean age (year) for different Δ/Γ ratios. The unity ratio of 1.0 is shown as a blue dashed line, and the lower and upper limits as solid magenta and black lines, respectively. The ratio of 0.6 is shown as a cyan solid line. The CFC-12 shows a distribution anomaly that is caused by the decreasing atmospheric concentration of CFC-12. (b) Average vertical profiles of mean age (year) versus potential density (kg/m^3) for the given Δ/Γ ratios. The ratio of 1.0 is shown as blue solid and dashed lines, the ratio of 0 is shown as magenta solid and dashed lines, and the ratio of 0.6 is shown as cyan solid and dashed lines. SSCS = southern South China Sea; LU = Luzon Strait; CFC = chlorofluorocarbon.

Considering that it is important to constrain the TTD shape, that is, Δ/Γ ratio, we now focus on the ratio smaller than one. For pure advection, that is, $\Delta/\Gamma = 0$, the mean age is equivalent to partial pressure age (Waugh et al., 2003). Figure 9b shows the estimated ages with Δ/Γ ratio from 0 to 1. As a result, for the same isopycnals (i.e., $26 < \sigma_\theta < 27$) an extremely short residence time range from 3 to 8 years can be obtained. Care must be taken that pure advection is not true for the real ocean; hence, this would be a lower limit of our age estimate. If we adjust Δ/Γ ratio, then the residence time results from ratio of 0.6 might be very close to the result of Liu and Gan. Nevertheless, we cannot draw any conclusion that this ratio of 0.6 must be an optimum one to represent the role of advection relative to diffusion. But it would be expected that lower age and transit time could be obtained and more practical.

4.4. Caveats for CFC-12 Application in This Study

At first, it is well known that the SCS is mainly located in the tropical zone; thus, the sea surface temperature is consistently high for all seasons (Chao et al., 1996). As a result, the upper water column is permanently well stratified (Shaw & Chao, 1994). In other words, there is no strong vertical convection process in winter time that could bring surface water down to the deep layer. Thus, the CFC-12 existed in the SCS must originate from the entrainment by the inflow across LU, and the tracer signal observed in the SCS interior is weaker than that in the WP. In this case, CFC-12 does not show apparent seasonal variation.

Observable seasonal change could be practical for the surface layer. The concentration of CFC-12 dissolved in the surface water is upon solubilities, atmospheric concentrations, and physical factors affecting the gas saturations, including seasonality upwelling and entrainment due to mixing (Fine, 2011). Thus, it is possible to seek annual or even shorter variation since the surface gas saturated condition and anomalies might be influenced by seasonality process. In this study, however, we mainly focus on the waters below the warm surface layer where CFC-12 data cannot track most useful information owing to its decline in atmosphere since mid-2000s.

Furthermore, as a time-varying chorological tracer, CFC-12 can enter the ocean interior continuously. That means the CFC-12 is an indicator that could highlight interior ocean region where surface-derived phenomenon could be transported on interannual to decadal time scales. Also, the mean age, determined from the TTD approach, represents the averaged age for the mixture of water parcel in the sample location in the ocean interior. Hence, a shorter time scale change cannot be captured especially for older intermediate water.

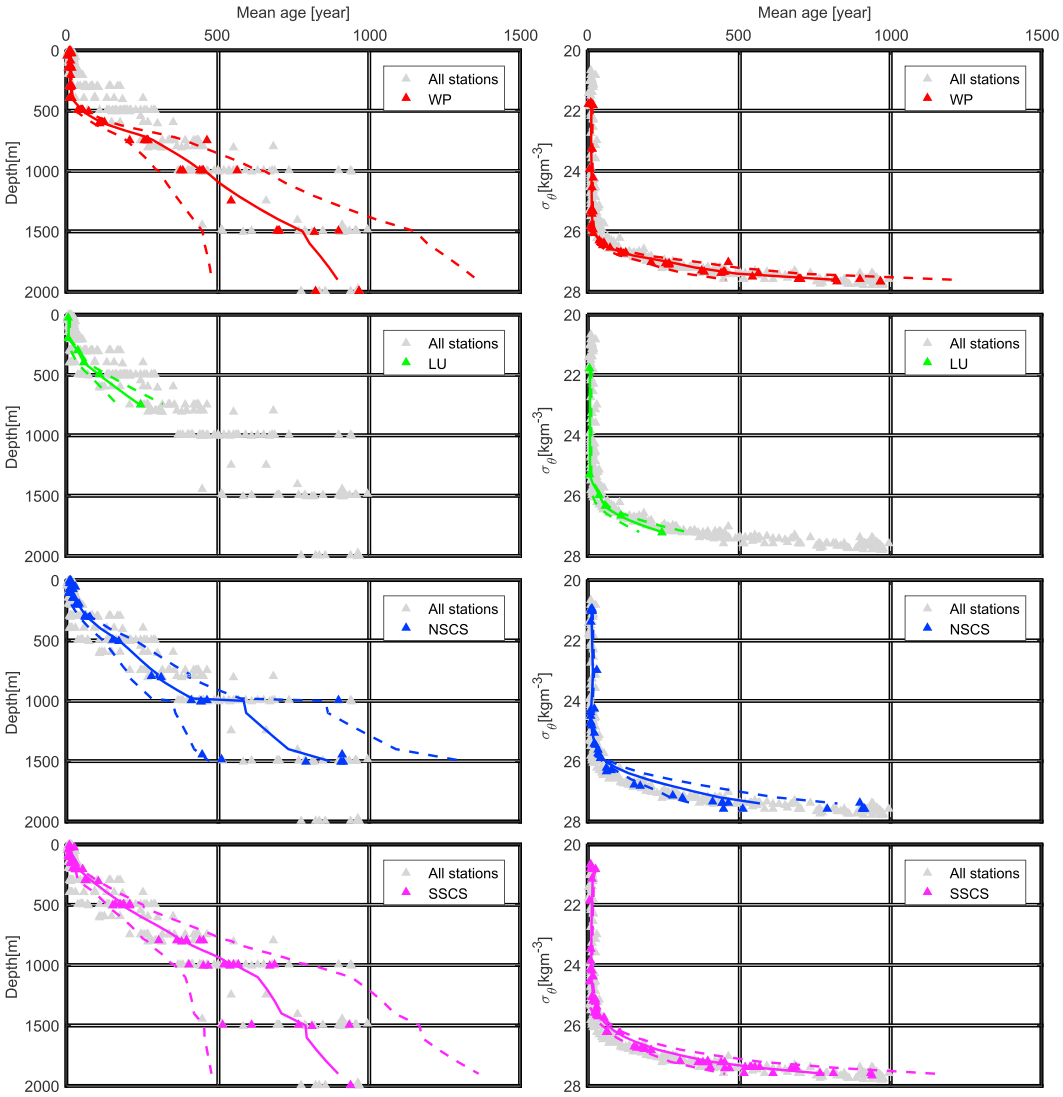

Figure 10. Profiles of all estimated mean ages (gray triangles) together with the average profiles of the mean age (solid lines) versus depth (left column) and potential density (right column). The dashed lines represent the analytical errors and the spatial variations. NSCS = northern South China Sea; SSCS = southern South China Sea; LU = Luzon Strait; WP = western Pacific.

As a result, CFC-12 could provide a path-integrated and averaged age information for study area. But a tracer such as SF_6, which is still increasing monotonically, might track newly ventilated water for the surface layer and could provide transient or in situ anomalies seasonally.

5. Conclusions

In this study, we present CFC-12 data in the SCS, LU, and WP during September and October 2016. The CFC-12, together with the oxygen and hydrographic data, is used to provide general picture of tracer distributions and ventilation time scale of the SCS, LU, and WP.

A CFC-12 maximum could be found around subsurface layer (150–200 m) in the SCS, while broaden in the WP to the depth of ~400 m. The maximum core could be tracked to the NPTW. Generally, the spatial CFC-12 distribution reveals a pronounced decrease westward across the LU and a slight decrease southward in the SCS. The oldest water in the SCS, which lies between the relatively young waters above and deep water below, could be tracked by the oxygen minimum in the intermediate waters. The CFC-12 and oxygen data are

used together as complementary tracers and identify the sandwiched structure vertically of the flows across the LU.

The mean age was calculated based on TTD approach to quantify ventilation time scale of waters. By comparing the water ages between the NSCS and the WP, we find that the LU acted as a transition zone in the upper several hundred meters (or $\sigma_\theta < 27$). In the LU, the mean age of the S_{min} water is 113 ± 31 years, though with large uncertainty. For the water deeper than 500 m, the mean ages continue to increase with depth until the value exceeded 400 years at ~1,000 m. Similarly, the mean age of the S_{min} water rapidly increases to 147 ± 41 years.

The mean age gradient of the S_{min} water must be the consequence of intensive mixing and entrainment of the inflow water from the WP. A similar tendency is also found in the stations along 10°N; the S_{min} water is 191 ± 53 years. An expected increase in age between the LU and SSCS is verified to reflect the transit time for the given water layers in the SCS. For the intermediate water ($26 < \sigma_\theta < 27$), the mean age differences range from 23 to 122 years. As a result, a mean transit time of 77 ± 20 years is estimated for the intermediate water in the SCS interior.

In brief, using the TTD-derived mean age with transient tracers provided a possible way to determine the path-integrated and averaged time scale for study area. To better constrain the TTD shape, that is, Δ/Γ ratio, simultaneous measurements of the CFCs and other transient tracers with different time scales and input functions, such as SF_6, ^{81}Kr, and ^{39}Ar, are essential for dating water movement and ventilation in the future. Also, a tracer such as SF_6, which is still increasing monotonically, could track newly ventilated water for the surface layer and could provide transient or in situ anomalies seasonally.

Acknowledgments
This work was supported by the National Natural Science Foundation of China (41776088, 40976113, 41076133, and 91228202), Fund of Key Laboratory of Global Change and Marine-Atmospheric Chemistry, State Oceanic Administration, China (GCMAC1404), Senior Project of Big Science Instrument Office, Institute of Oceanology, Chinese Academy of Sciences (KEXUE2016G01 and KEXUE2017G09), the Natural Science Foundation of Fujian Province, China (2014J06014), Xiamen University Training Program of Innovation and Entrepreneurship for Undergraduates (2016X0619 and 2016X0624), and the Basal Research Fund of Xiamen University. We thank the captains, crews, and scientists aboard the RV SHIYAN I, led by chief scientist Huabin Mao, and the RV KEXUE, led by chief scientist Hui Zhou, for their support during the cruises. Many thanks to Xianghui Guo, Kaiwen Shi, Chao Wang, Zhiheng Wang, Guowen Tang, Zhai Wu, Zhentong Yao, and Xibao Su for their help with sampling. All the data used in this study are listed in the Data Set S1.

References

Beining, P., & Roether, W. (1996). Temporal evolution of CFC 11 and CFC 12 concentrations in the ocean interior. *Journal of Geophysical Research*, *101*, 16,455–16,464. https://doi.org/10.1029/96JC00987

Broecker, W. S., Patzert, W. C., Toggweiler, J. R., & Stuiver, M. (1986). Hydrography, chemistry, and radioisotopes in the Southeast-Asian basins. *Journal of Geophysical Research*, *91*, 14,345–14,354. https://doi.org/10.1029/JC091ic12p14345

Bullister, J. L. (2015). Atmospheric histories (1765–2015) for CFC-11, CFC-12, CFC-113, CCl_4, SF_6 and N_2O, NDP-095. Carbon Dioxide Inf. Anal. Cent., Oak Ridge Natl. Lab., US Dep. of Energy, Oak Ridge, TN. https://doi.org/10.3334/CDIAC/otg. CFC_ATM_Hist_2015. Retrieved from http://cdiac. ornl.gov/ftp/oceans/CFC_ATM_Hist/CFC_ATM_Hist_2015

Bullister, J. L., Wisegarver, D. P., & Menzia, F. A. (2002). The solubility of sulfur hexafluoride in water and seawater. *Deep Sea Research Part I: Oceanographic Research Papers*, *49*(1), 175–187. https://doi.org/10.1016/S0967-0637(01)00051-6

Busenberg, E., & Plummer, L. N. (1992). Use of chlorofluorocarbons (Ccl3f and Ccl2f2) as hydrologic tracers and age-dating tools—The alluvium and terrace system of Central Oklahoma. *Water Resources Research*, *28*, 2257–2283. https://doi.org/10.1029/92WR01263

Cai, M. G., Deng, H. X., Huang, P., Ke, H. W., Zheng, X. H., & Li, W. Q. (2016). Simultaneous determination of chlorofluorocarbons and sulfur hexafluoride in seawater based on a purge and trap gas chromatographic system. *Chinese Journal of Analytical Chemistry*, *44*(7), 1003–1008. https://doi.org/10.1016/S1872-2040(16)60941-6

Cai, M. G., Lin, Y., Chen, M., Yang, W. F., Du, H. H., Xu, Y., et al. (2017). Improved source apportionment of PAHs and Pb by integrating Pb stable isotopes and positive matrix factorization application (PAHs): A historical record case study from the northern South China Sea. *Science of the Total Environment*, *609*, 577–586. https://doi.org/10.1016/j.scitotenv.2017.07.190

Chang, Y. T., Hsu, W. L., Tai, J. H., Tang, T. Y., Chang, M. H., & Chao, S. Y. (2010). Cold deep water in the South China Sea. *Journal of Oceanography*, *66*(2), 183–190. https://doi.org/10.1007/s10872-010-0016-x

Chao, S. Y., Shaw, P. T., & Wu, S. Y. (1996). Deep water ventilation in the South China Sea. *Deep Sea Research Part I: Oceanographic Research Papers*, *43*(4), 445–466. https://doi.org/10.1016/0967-0637(96)00025-8

Chen, C. T. A., & Huang, M. H. (1996). A mid-depth front separating the South China Sea water and the Philippine Sea water. *Journal of Oceanography*, *52*(1), 17–25. https://doi.org/10.1007/BF02236530

Chen, C. T. A., Wang, S. L., Chou, W. C., & Sheu, D. D. (2006). Carbonate chemistry and projected future changes in pH and $CaCO_3$ saturation state of the South China Sea. *Marine Chemistry*, *101*(3–4), 277–305. https://doi.org/10.1016/j.marchem.2006.01.007

Chen, C. T. A., Wang, S. L., Wang, B. J., & Pai, S. C. (2001). Nutrient budgets for the South China Sea basin. *Marine Chemistry*, *75*(4), 281–300. https://doi.org/10.1016/S0304-4203(01)00041-X

Chu, P. C., Edmons, N. L., & Fan, C. W. (1999). Dynamical mechanisms for the South China Sea seasonal circulation and thermohaline variabilities. *Journal of Physical Oceanography*, *29*(11), 2971–2989. https://doi.org/10.1175/1520-0485(1999)029<2971:dmftsc>2.0.co;2

Chu, P. C., & Li, R. F. (2000). South China Sea isopycnal-surface circulation. *Journal of Physical Oceanography*, *30*(9), 2419–2438. https://doi.org/10.1175/1520-0485(2000)030<2419:scsisc>2.0.co;2

Dai, M. H., Meng, F. F., Tang, T. T., Kao, S. J., Lin, J. R., Chen, J. H., et al. (2009). Excess total organic carbon in the intermediate water of the South China Sea and its export to the North Pacific. *Geochemistry, Geophysics, Geosystems*, *10*, Q12002. https://doi.org/10.1029/2009GC002752

Deng, H. X., Ke, H. W., Huang, P., Chen, X. D., & Cai, M. G. (2018). Ventilation time and anthropogenic CO_2 in the Bering Sea and the Arctic Ocean based on carbon tetrachloride measurements. *Journal of Oceanography*. https://doi.org/10.1007/s10872-018-0471-3

Fang, G. H., Wang, Y. G., Wei, Z. X., Fang, Y., Qiao, F. L., & Hu, X. M. (2009). Interocean circulation and heat and freshwater budgets of the South China Sea based on a numerical model. *Dynamics of Atmospheres and Oceans*, *47*(1–3), 55–72. https://doi.org/10.1016/j.dynatmoce.2008.09.003

Fieux, M., Andrie, C., & Charriaud, A. G. (1996). Hydrological and chlorofluoromethane measurements of the Indonesian throughflow entering the Indian Ocean. *Journal of Geophysical Research*, *101*, 12,433–12,454. https://doi.org/10.1029/96JC00207

Fine, R. A. (2011). Observations of CFCs and SF_6 as ocean tracers. *Annual Review of Marine Science*, *3*(1), 173–195. https://doi.org/10.1146/annurev.marine.010908.163933

Gong, G. C., Liu, K. K., Liu, C. T., & Pai, S. C. (1992). The chemical hydrography of the South China Sea west of Luzon and a comparison with the West Philippine Sea. *Terrestrial, Atmospheric and Oceanic Sciences*, *3*(4), 587–602. https://doi.org/10.3319/TAO.1992.3.4.587(O)

Gruber, N., Sarmiento, J. L., & Stocker, T. F. (1996). An improved method for detecting anthropogenic CO_2 in the oceans. *Global Biogeochemical Cycles*, *10*, 809–837. https://doi.org/10.1029/96GB01608

Hartin, C. A., Fine, R. A., Sloyan, B. M., Talley, L. D., Chereskin, T. K., & Happell, J. (2011). Formation rates of Subantarctic mode water and Antarctic intermediate water within the South Pacific. *Deep Sea Research Part I: Oceanographic Research Papers*, *58*(5), 524–534. https://doi.org/10.1016/j.dsr.2011.02.010

Huang, P., & Tanhua, T. (2017). Ventilation and anthropogenic CO_2 in the Sulu Sea. *Journal of Marine Systems*, *170*, 1–9. https://doi.org/10.1016/j.jmarsys.2017.01.014

Huang, P., Zhang, M. M., Cai, M. G., Ke, H. W., Deng, H. X., & Li, W. Q. (2016). Ventilation time and anthropogenic CO2 in the South China Sea based on CFC-11 measurements. *Deep Sea Research Part I: Oceanographic Research Papers*, *116*, 187–199. https://doi.org/10.1016/j.dsr.2016.08.006

Khatiwala, S., Tanhua, T., Fletcher, S. M., Gerber, M., Doney, S. C., Graven, H. D., et al. (2012). Global ocean storage of anthropogenic carbon. *Biogeosciences*, *10*(4), 2169–2191. https://doi.org/10.5194/bg-10-2169-2013

LeBel, D. A., Smethie, W. M., Rhein, M., Kieke, D., Fine, R. A., Bullister, J. L., et al. (2008). The formation rate of North Atlantic Deep Water and Eighteen Degree Water calculated from CFC-11 inventories observed during WOCE. *Deep Sea Research Part I: Oceanographic Research Papers*, *55*(8), 891–910. https://doi.org/10.1016/j.dsr.2008.03.009

Li, F. Q., Li, L., Wang, X. Q., & Liu, C. L. (2002). Water masses in the South China Sea and water exchange between the Pacific and the South China Sea. *Journal of Ocean University of China*, *1*(1), 19–24. https://doi.org/10.1007/s11802-002-0025-5

Li, L., & Qu, T. D. (2006). Thermohaline circulation in the deep South China Sea basin inferred from oxygen distributions. *Journal of Geophysical Research*, *111*, C05017. https://doi.org/10.1029/2005JC003164

Liu, Z., & Gan, J. (2017). Three-dimensional pathways of water masses in the South China Sea: A modeling study. *Journal of Geophysical Research: Oceans*, *122*, 6039–6054. https://doi.org/10.1002/2016JC012511

Liu, Q. Y., Yang, H. J., & Liu, Z. Y. (2001). Seasonal features of the Sverdrup circulation in the South China Sea. *Progress in Natural Science*, *11*(3), 202–206.

Liu, T. Y., Xu, J. X., He, Y. H., Lu, H. B., Yao, Y., & Cai, S. Q. (2016). Numerical simulation of the Kuroshio intrusion into the South China Sea by a passive tracer. *Acta Oceanologica Sinica*, *35*(9), 1–12. https://doi.org/10.1007/s13131-016-0930-x

Mecking, S., Warner, M. J., Greene, C. E., Hautala, S. L., & Sonnerup, R. E. (2004). Influence of mixing on CFC uptake and CFC ages in the North Pacific thermocline. *Journal of Geophysical Research*, *109*, C07014. https://doi.org/10.1029/2003JC001988

Nitani, H. (1972). Beginning of the Kuroshio. In H. Stommel & K. Yashida (Eds.), *Kuroshio, physical aspects of the Japan Current* (pp. 129–163). Seattle: University of Washington Press.

Orsi, A. H., Johnson, G. C., & Bullister, J. L. (1999). Circulation, mixing, and production of Antarctic Bottom Water. *Progress in Oceanography*, *43*(1), 55–109. https://doi.org/10.1016/S0079-6611(99)00004-X

Qu, T. D. (2000). Upper-layer circulation in the South China Sea. *Journal of Physical Oceanography*, *30*(6), 1450–1460. https://doi.org/10.1175/1520-0485(2000)030<1450:ULCITS>2.0.CO;2

Qu, T. D. (2002). Evidence for water exchange between the South China Sea and the Pacific Ocean through the Luzon Strait. *Acta Oceanologica Sinica*, *21*(2), 175–185.

Qu, T. D., Girton, J. B., & Whitehead, J. A. (2006). Deepwater overflow through Luzon Strait. *Journal of Geophysical Research*, *111*, C01002. https://doi.org/10.1029/2005JC003139

Qu, T. D., & Lindstrom, E. J. (2004). Northward intrusion of Antarctic Intermediate Water in the western Pacific. *Journal of Physical Oceanography*, *34*(9), 2104–2118. https://doi.org/10.1175/1520-0485(2004)034<2104:NIOAIW>2.0.CO;2

Qu, T. D., Mitsudera, H., & Yamagata, T. (1999). A climatology of the circulation and water mass distribution near the Philippine coast. *Journal of Physical Oceanography*, *29*(7), 1488–1505. https://doi.org/10.1175/1520-0485(1999)029<1488:ACOTCA>2.0.CO;2

Qu, T. D., Mitsudera, H., & Yamagata, T. (2000). Intrusion of the North Pacific waters into the South China Sea. *Journal of Geophysical Research*, *105*, 6415–6424. https://doi.org/10.1029/1999JC900323

Qu, T. D., Song, Y. T., & Yamagata, T. (2009). An introduction to the South China Sea throughflow: Its dynamics, variability, and application for climate. *Dynamics of Atmospheres and Oceans*, *47*(1–3), 3–14. https://doi.org/10.1016/j.dynatmoce.2008.05.001

Rhein, M. (1994). The deep western boundary current—Tracers and velocities. *Deep Sea Research Part I: Oceanographic Research Papers*, *41*(2), 263–281. https://doi.org/10.1016/0967-0637(94)90003-5

Rhein, M., Fischer, J., Smethie, W. M., Smythe-Wright, D., Weiss, R. F., Mertens, C., et al. (2002). Labrador Sea Water: Pathways, CFC inventory, and formation rates. *Journal of Physical Oceanography*, *32*(2), 648–665. https://doi.org/10.1175/1520-0485(2002)032<0648:Lswpci>2.0.Co;2

Sabine, C. L., Feely, R. A., Gruber, N., Key, R. M., Lee, K., Bullister, J. L., et al. (2004). The oceanic sink for anthropogenic CO_2. *Science*, *305*(5682), 367–371. https://doi.org/10.1126/science.1097403

Schlitzer, R. (2017). Ocean Data View. Retrieved from https://odv.awi.de

Shaw, P. T., & Chao, S. Y. (1994). Surface circulation in the South China Sea. *Deep Sea Research Part I: Oceanographic Research Papers*, *41*(11-12), 1663–1683. https://doi.org/10.1016/0967-0637(94)90067-1

Shaw, P. T., Chao, S. Y., & Fu, L. L. (1999). Sea surface height variations in the South China Sea from satellite altimetry. *Oceanologica Acta*, *22*(1), 1–17. https://doi.org/10.1016/s0399-1784(99)80028-0

Smethie, M., Fine, A., Putzka, A., & Jones, E. P. (2000). Tracing the flow of North Atlantic Deep Water using chlorofluorocarbons. *Journal of Geophysical Research*, *105*, 14,297–14,323. https://doi.org/10.1029/1999JC900274

Smethie, W. M., & Fine, R. A. (2001). Rates of North Atlantic Deep Water formation calculated from chlorofluorocarbon inventories. *Deep Sea Research Part I: Oceanographic Research Papers*, *48*(1), 189–215. https://doi.org/10.1016/S0967-0637(00)00048-0

Sonnerup, R. E., Bullister, J. L., & Warner, M. J. (2008). Improved estimates of ventilation rate changes and CO_2 uptake in the Pacific Ocean using chlorofluorocarbons and sulfur hexafluoride. *Journal of Geophysical Research*, *113*, C12007. https://doi.org/10.1029/2008JC004864

Sonnerup, R. E., Quay, P. D., & Bullister, J. L. (1999). Thermocline ventilation and oxygen utilization rates in the subtropical North Pacific based on CFC distributions during WOCE. *Deep Sea Research Part I: Oceanographic Research Papers*, *46*(5), 777–805. https://doi.org/10.1016/s0967-0637(98)00092-2

Stöven, T. (2011). Ventilation Processes of the Mediterranean Sea based on CFC-12 and SF6 measurements, (Diploma thesis, 152 pp.). Christian-Albrechts-Universität.

Suga, T., Kato, A., & Hanawa, K. (2000). North Pacific Tropical Water: Its climatology and temporal changes associated with the climate regime shift in the 1970s. *Progress in Oceanography*, *47*(2-4), 223–256. https://doi.org/10.1016/S0079-6611(00)00037-9

Sun, N. (2006). Distribution of chlorofluorocarbon and its tracer study of water masses in the Arctic Ocean, Bering Sea and the southern South China Sea, (Doctoral thesis, 169 pp.). Xiamen University.

Tanhua, T., Jones, E. P., Jeansson, E., Jutterström, S., Smethie, W. M., Wallace, D. W. R., & Anderson, L. G. (2009). Ventilation of the Arctic Ocean: Mean ages and inventories of anthropogenic CO_2 and CFC-11. *Journal of Geophysical Research*, *114*, C01002. https://doi.org/10.1029/2008JC004868

Tanhua, T., & Liu, M. (2015). Upwelling velocity and ventilation in the Mauritanian upwelling system estimated by CFC-12 and SF_6 observations. *Journal of Marine Systems*, *151*, 57–70. https://doi.org/10.1016/j.jmarsys.2015.07.002

Tanhua, T., Waugh, D. W., & Wallace, D. W. (2008). Use of SF_6 to estimate anthropogenic CO_2 in the upper ocean. *Journal of Geophysical Research*, *113*, C04037. https://doi.org/10.1029/2007JC004416

Tian, J. W., Yang, Q. X., Liang, X. F., Xie, L. L., Hu, D. X., Wang, F., & Qu, T. D. (2006). Observation of Luzon Strait transport. *Geophysical Research Letters*, *33*, L19607. https://doi.org/10.1029/2006GL026272

Tian, J. W., Yang, Q. X., & Zhao, W. (2009). Enhanced diapycnal mixing in the South China Sea. *Journal of Physical Oceanography*, *39*(12), 3191–3203. https://doi.org/10.1175/2009JPO3899.1

Vollmer, M. K., & Weiss, R. F. (2002). Simultaneous determination of sulfur hexafluoride and three chlorofluorocarbons in water and air. *Marine Chemistry*, *78*(2–3), 137–148. https://doi.org/10.1016/s0304-4203(02)00015-4

Wang, G., Xie, S. P., Qu, T., & Huang, R. X. (2011). Deep South China Sea circulation. *Geophysical Research Letters*, *38*, L05601. https://doi.org/10.1029/2010GL046626

Wang, J. (1986). Observation of abyssal flows in the northern South China Sea. *Acta Oceanographica Taiwanica*, *16*, 36–45.

Wang, X. W., Liu, Z. Y., & Peng, S. Q. (2017). Impact of tidal mixing on water mass transformation and circulation in the South China Sea. *Journal of Physical Oceanography*, *47*(2), 419–432. https://doi.org/10.1175/Jpo-D-16-0171.1

Warner, M. J., Bullister, J. L., Wisegarver, D. P., Gammon, R. H., & Weiss, R. F. (1996). Basin-wide distributions of chlorofluorocarbons CFC-11 and CFC-12 in the North Pacific: 1985-1989. *Journal of Geophysical Research*, *101*, 20,525–20,542. https://doi.org/10.1029/96JC01849

Warner, M. J., & Weiss, R. F. (1985). Solubilities of chlorofluorocarbons 11 and 12 in water and seawater. *Deep Sea Research Part I: Oceanographic Research Papers*, *32*(12), 1485–1497. https://doi.org/10.1016/0198-0149(85)90099-8

Warn-Varnas, A., Hawkins, J., Lamb, K. G., Piacsek, S., Chin-Bing, S., King, D., & Burgos, G. (2010). Solitary wave generation dynamics at Luzon Strait. *Ocean Modelling*, *31*(1–2), 9–27. https://doi.org/10.1016/j.ocemod.2009.08.002

Waugh, D., Hall, T., McNeil, B., Key, R., & Matear, R. (2006). Anthropogenic CO_2 in the oceans estimated using transit time distributions. *Tellus B*, *58*(5), 376–389. https://doi.org/10.1111/j.1600-0889.2006.00222.x

Waugh, D. W., Haine, T. W. N., & Hall, T. M. (2004). Transport times and anthropogenic carbon in the subpolar North Atlantic Ocean. *Deep Sea Research Part I: Oceanographic Research Papers*, *51*(11), 1475–1491. https://doi.org/10.1016/j.dsr.2004.06.011

Waugh, D. W., Hall, T. M., & Haine, T. W. N. (2003). Relationships among tracer ages. *Journal of Geophysical Research*, *108*(C5), 3138. https://doi.org/10.1029/2002JC001325

Waworuntu, J. M., Fine, R. A., Olson, D. B., & Gordon, A. L. (2000). Recipe for Banda Sea water. *Journal of Marine Research*, *58*(4), 547–569. https://doi.org/10.1357/002224000321511016

Wu, K., Dai, M. H., Chen, J. H., Meng, F. F., Li, X. L., Liu, Z. Y., et al. (2015). Dissolved organic carbon in the South China Sea and its exchange with the western Pacific Ocean. *Deep-Sea Research Part II: Topical Studies in Oceanography*, *122*, 41–51. https://doi.org/10.1016/j.dsr2.2015.06.013

Wyrtki, K. (1961). Scientific results of marine investigations of the South China Sea and the Gulf of Thailand 1959-1961: Physical oceanography of the Southeast Asian waters (Naga Rep. 2, 195 pp.). Scripps Inst. Of Oceanogr., La Jolla, CA.

Xu, F. H., & Oey, L. Y. (2014). State analysis using the local ensemble transform Kalman filter (LETKF) and the three-layer circulation structure of the Luzon Strait and the South China Sea. *Ocean Dynamics*, *64*(6), 905–923. https://doi.org/10.1007/s10236-014-0720-y

Xu, F. H., & Oey, L. Y. (2015). Seasonal SSH variability of the northern South China Sea. *Journal of Physical Oceanography*, *45*(6), 1595–1609. https://doi.org/10.1175/jpo-d-14-0193.1

Xue, H. J., Chai, F., Pettigrew, N., Xu, D. Y., Shi, M., & Xu, J. P. (2004). Kuroshio intrusion and the circulation in the South China Sea. *Journal of Geophysical Research*, *109*, C02017. https://doi.org/10.1029/2002JC001724

Yang, Q. X., Tian, J. W., & Zhao, W. (2011). Observation of material fluxes through the Luzon Strait. *Chinese Journal of Oceanology and Limnology*, *29*(1), 26–32. https://doi.org/10.1007/s00343-011-9952-6

Yaremchuk, M., McCreary, J., Yu, Z. J., & Furue, R. (2009). The South China Sea throughflow retrieved from climatological data. *Journal of Physical Oceanography*, *39*(3), 753–767. https://doi.org/10.1175/2008JPO3955.1

You, Y. Z., Chern, C. S., Yang, Y., Liu, C. T., Liu, K. K., & Pai, S. C. (2005). The South China Sea, a cul-de-sac of North Pacific Intermediate Water. *Journal of Oceanography*, *61*(3), 509–527. https://doi.org/10.1007/s10872-005-0059-6

Zeng, L., Wang, D., Xiu, P., Shu, Y., Wang, Q., & Chen, J. (2016). Decadal variation and trends in subsurface salinity from 1960 to 2012 in the northern South China Sea. *Geophysical Research Letters*, *43*, 12,181–12,189. https://doi.org/10.1002/2016GL071439

Zhao, W., Zhou, C., Tian, J. W., Yang, Q. X., Wang, B., Xie, L. L., & Qu, T. D. (2014). Deep water circulation in the Luzon Strait. *Journal of Geophysical Research: Oceans*, *119*, 790–804. https://doi.org/10.1002/2013JC009587